STUDY OF SEISMIC DATA FROM THE CADÍ (LEGEF-IEC) BROADBAND STATION

Júlia Ladero Gálvez
Facultat de Física, Universitat de Barcelona, Diagonal 645, 08028 Barcelona, Spain.

Advisors: Emma Suriñach, Mar Tapia

Abstract: Verifying the quality of data recorded by seismic stations is essential, particularly when the station is part of a broader seismic network. In this study, we assess the data quality of the Cadí (LEGEC-IEC) broadband station. This evaluation is conducted through the elaboration, analysis, and comparison of cumulative Power Spectral Density (PSD) spectra, Root Mean Square (RMS) amplitude values, and the examination of various seismic events. The results indicate that the recorded data exhibits expected seasonal and frequency-dependent patterns, the ambient noise levels are within acceptable limits, and the station reliably captures global seismic events. Consequently, we conclude that the data produced by the station is of high quality and temporally consistent; therefore, the station is operating correctly.
Keywords: seismology, broadband, data analysis, data filtering
SDGs: This work is related to Sustainable Development Goal 13

I. INTRODUCTION

Seismic stations consist of a signal digitizer, a three-component seismometer, a connection to the internet to get the time, and a power supply. The association of seismic stations forms a seismic network, which can be local or global (for example, the Catalan Seismic Network, CA, or the Spanish Seismic Network, ES).

The Cadí broadband station is integrated into these networks, making the assessment of its data quality essential. This can be achieved by analyzing cumulative power spectral densities (PSD) and the root mean square (RMS) amplitude plots, as well as by comparing the station's recordings of selected seismic events with those from other stations.

II. CADÍ STATION

The Cadí station, owned, deployed, and maintained by LEGEF-IEC, is located inside the old Cadí Tunnel in the province of Lleida, at coordinates 42.3393 N and 1.8348 E. The Cadí station has both broadband and narrowband instrumentation.

Broadband stations are generally more suitable for global seismic events, while narrowband stations typically monitor regional or local activity. Seismic sensors may be velocimeters or accelerometers: accelerometers have a larger dynamic range and are more suitable for high-amplitude motions, which can clip on velocimeters; however, velocimeters detect low-amplitude signals more effectively. With appropriate data processing techniques, both types of sensors can now be used equally.

The broadband is equipped with a Guralp CMT-40T sensor, a Centaur digitizer, and a connection to the internet to get the time. The velocimeter features a 60 s long-period corner, a 100 Hz sampling rate (thus a 50 Hz Nyquist frequency), and 800 V/m/s sensitivity. The digitizer provides three channels, corresponding to the vertical, N-S, and E-W components of ground motion. The narrowband, a low-cost alternative, is a Raspberry Shake RS3D 3-channel plug-and-go seismograph. The velocimeter features a 2 s long-period corner, a 100 Hz sampling rate (thus a 50 Hz Nyquist frequency), and 108 V/m/s sensitivity. In October 2024, the narrowband station suffered a cessation of operation caused by electrical problems, but it was fixed recently.

III. DATA

The data analyzed, provided in MiniSEED format, correspond to the period from September 18, 2024, to April 30, 2025, for the broadband station. To enhance the seismic site characterization, this data was compared with a co-located narrowband station during the interval from September 12, 2024, to October 28, 2024.

IV. METHODOLOGY

It is noteworthy that this study primarily focuses on the vertical (Z) component of the data, as the horizontal components are more susceptible to wind-induced vibrations.

A. PSD

PSDs represent the quantification of seismic noise in a certain location over a specific period of time. The function, computed as the Fourier transform of the squared signal amplitude, has dimensions of decibels of power per Hz, enabling comparison of the location noise with the standard new low noise model (NLNM) and new high noise model (NHNM) curves initially established by Peterson in 1993 [2] and later refined by McNamara in 2004 [1]. An example of a PSD plot is displayed in Figure 1.

PSDs usually present characteristic windows or peaks. For instance, the peak between 1 and 10 Hz reflects global

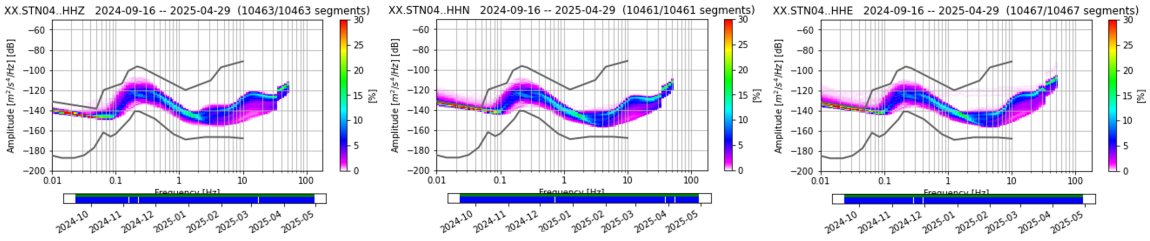

FIG. 1: Cumulative PSD spectra expressed in % for the Z, N, and E components for the whole data analyzed, from 2024-09-16 to 2025-04-29. The grey curves are PSD spectra of the Earth's ambient seismic noise from [1]: upper (noisy) and lower (quiet). Data are expressed as dB relative to 1 m^2 s^{-4} Hz^{-1}.

oceanic oscillations, and it is also related to meteorology and thus exhibits seasonal variability.

In order to assess the quality of the seismic station, two approaches were taken: a probabilistic one via the cumulative PSDs and a quantitative one. The cumulative PSDs analysis verifies that the station's noise levels lie between the NLNM and NHNM. It also provides an insight into the station's detection range. The analysis of quantitative information, such as RMS amplitude extracted from the PSDs, is a study of the station's background noise response, serving as a characterization of its baseline quality.

B. PSD and RMS amplitude data treatment

The processing of the data given by the seismic station is made up of 2 stages: the pre-processing of the data and the actual processing of the data.

Pre-processing of the data consists of the instrumental deconvolution, which allows recovery of the true ground motion. In such a process, the data undergoes a conversion first from volts to digital counts (digitizer) and then from digital counts to physical units (via the sensor), such as velocity, acceleration, or displacement. In this particular case, acceleration was selected as the output parameter. No additional filters or corrections were applied at this stage.

The processing of the data consists of the computing of the PSD in two forms, the first one being cumulative PSDs, as in McNamara [1], which is the probability density function of the PSD collection, and RMS amplitude. Regarding the former analysis, several samplings were made, those being the full data set, seasonal, and monthly. The latter was examined through both linear and polar plots. Additionally, data were sorted by day of the week to enable comparison with a recent study of Catalan seismic stations [3].

Finally, the RMS amplitude of the PSD was computed. To do so, adapted scripts from SeismoRMS [4] were used, available through GitHub. SeismoRMS is a Python-based software that utilizes routines from the ObsPy package to compute, store, and visually represent seismic background noise in terms of ground motion acceleration across specific frequency bands.

C. Seismology

A seismic event is a sudden release of energy from a seismic source, such as an earthquake, explosion, snowslide, etc. These recordings of ground motion are reflected in seismograms. In the analysis of earthquake displays, three primary wave types are observed: P-waves, S-waves, and surface waves. P-waves are compressional and travel the fastest, hence the designation "primary waves", as they arrive first. S-waves are slower shear waves, while surface waves propagate along the Earth's surface and always arrive subsequent to S-waves [5] [6].

Earthquakes are generally classified as local, regional, or teleseismic. Local events occur within approximately 100 km of the station and primarily exhibit P and S waves. Regional earthquakes, occurring between 100 and 1000 km, also present surface waves. Teleseismic events, located beyond 1000 km, also generate pronounced surface waves alongside P and S waves. Detection of seismic events depends on frequency bands: local earthquakes produce higher-frequency signals above 1 Hz, regional events occupy the mid-frequency range of 0.1 to 5 Hz, and teleseismic events are dominant in the low-frequency band below 0.1 Hz.

To verify the reliability of the station, recordings of local, regional, and teleseismic events will be analyzed and compared with the narrowband station and other CA network stations.

D. Data treatment of seismological events

The previous pre-processing methodology was employed, with velocity selected as the output variable to improve the clarity of the visual representations.

Regarding the actual processing of the data, a classical approach was adopted: a water level was first applied, followed by filtering to isolate and better visualize the relevant seismic signals.

V. RESULTS

A. Cumulative PSDs

Figure 1 presents a comparison of the Z, N, and E components for the complete dataset recorded by the

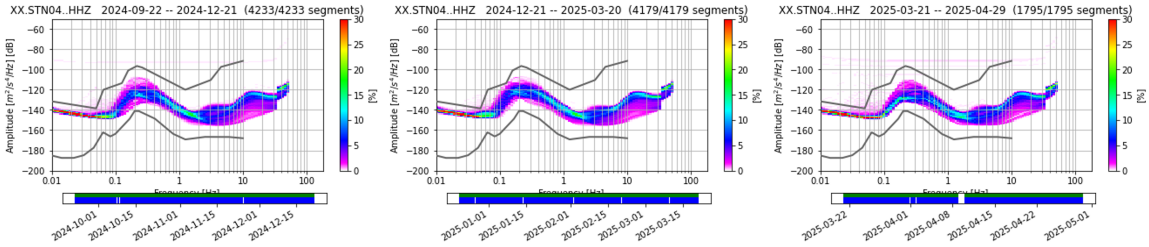

FIG. 2: Cumulative PSD spectra expressed in % for the Z component. Every graphic corresponds to one season: autumn, winter, and spring, respectively. The grey curves are PSD spectra of the Earth's ambient seismic noise from [1]: upper (noisy) and lower (quiet). Data are expressed as dB relative to 1 m^2 s^{-4} Hz^{-1}..

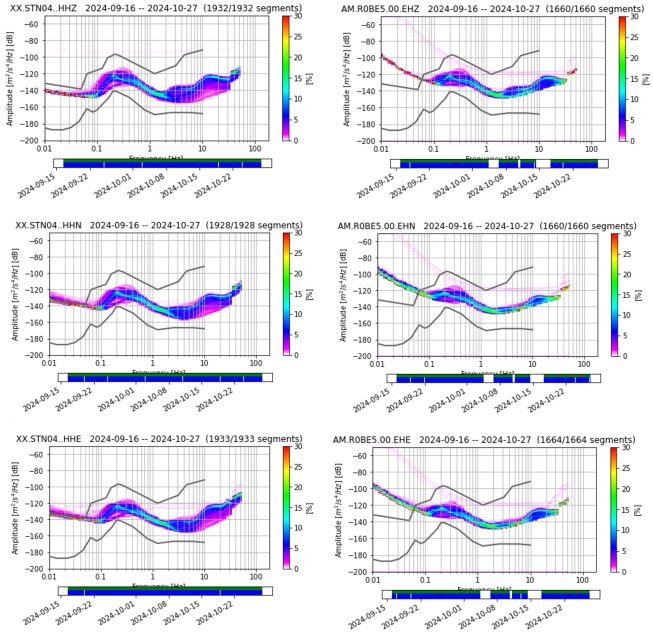

FIG. 3: Cumulative PSD spectra expressed in % for the Z, N, and E components. The left side represents the Guralp broadband station, and the right side the Raspberry station. Frequencies below 0.1 Hz cannot be compared since the Raspberry station is not broadband. The grey curves are PSD spectra of the Earth's ambient seismic noise from [1]: upper (noisy) and lower (quiet). Data are expressed as dB relative to 1 m^2 s^{-4} Hz^{-1}..

Guralp broadband station. Across all three components, the signal appears notably flat below 0.1 Hz, which may indicate an electronic limitation. Upon reviewing the sensor specifications, it is evident that the Guralp CMT-40T sensor is not true broadband and begins reliably detecting signals at approximately 0.03 Hz. In the figure, the signal becomes appreciable from around 0.05 Hz, as indicated by the broadening of the blue zone. Above 1 Hz, all components exhibit the characteristic shape of the NLNM and NHNM and fall within its range. As expected, the horizontal components (E and N) display greater variability, primarily due to wind-induced noise, which results in a broader data band. As a comparison with the PSD plots in [3], the spectral curves are consistent from 0.05 Hz and above.

Figure 2 displays a seasonal comparison of the PSD for the vertical component. The 0.1-1 Hz frequency band is of particular interest, as it reflects atmospheric variations and oceanic oscillations. Notably, the peak density in spring at 0.2 Hz (-130 dB) is lower than in autumn (-122 dB) and winter (-120 dB), seasons typically associated with more turbulent weather, which results in higher amplitude peaks. Above 1 Hz, a wider pink region is observed in winter, commonly linked to storm activity, an observation consistent with seasonal weather patterns. The horizontal components are available in the annex, along with monthly PSD plots for more detailed analysis.

Figure 3 presents a comparison between the Guralp broadband station and the Raspberry Shake. Frequencies below 0.1 Hz are excluded, as the Raspberry station lacks broadband capabilities. Nevertheless, both stations exhibit a similar spectral curve and have similar highs and lows and similar peak and trough patterns across the remaining frequency range.

B. Temporal evolution of seismic noise displacement

Figure 4 illustrates the variation in seismic noise displacement for the Z component across both the high- and low-frequency ends of the spectrum. In the high-frequency band, 10-40 Hz, the signal clearly reflects anthropogenic noise: average displacement values are higher on weekdays (approximately 0.3 mm) and lower on weekends (around 0.17 mm), consistent with human activity patterns previously described by Diaz et al. [3] for the CA seismic network. In contrast, the low-frequency band, 0.1-1 Hz, does not show the weekday–weekend distinction but instead reflects weather-related influences, as also observed in other CA seismic network stations [3]. During the winter months (November to March), average displacement values increase significantly. A smoothed version of the red line would show winter displacements frequently exceeding 600 nm, while values at either end of the timeline generally range between 200 and 400 nm. Specific peaks in late November, mid-to-late December, and late February align with significant storm and precipitation events reported by MeteoCat bulletins

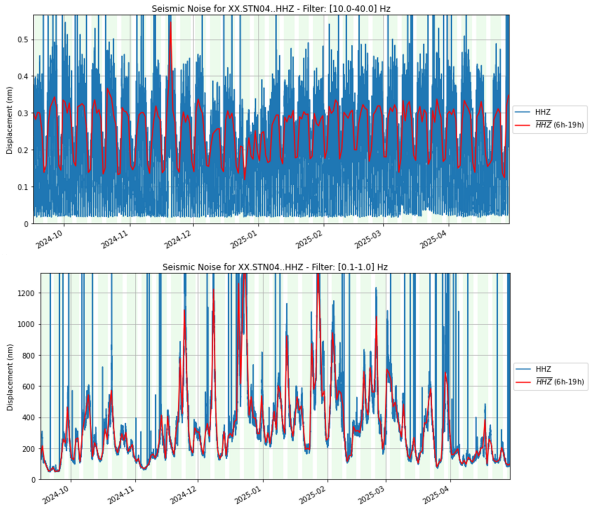

FIG. 4: Variations of the seismic noise displacement of the Z component of the Cadí station for the 0.1-1 Hz frequency band (above) and 10-40 Hz (below). Blue line: displacement value averaged every 30 minutes. Red line: daily averaged working and commuting hours (6h-19h UTC). Green strips indicate weekdays, and white strips weekends.

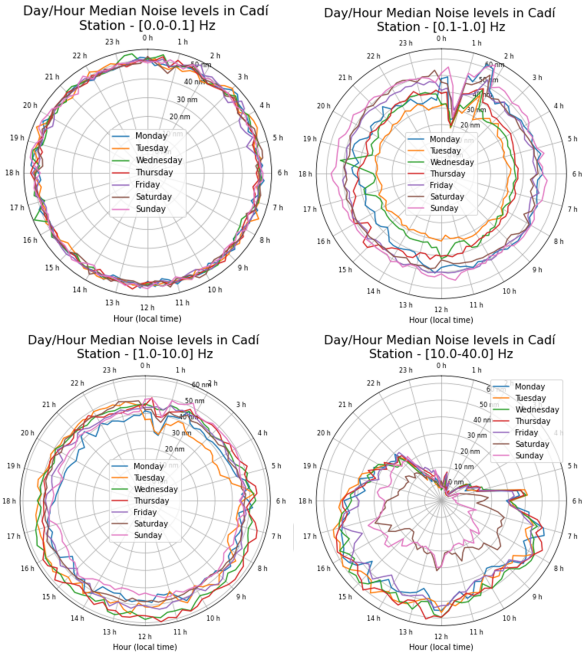

FIG. 5: Power amplitude variation averaged for each day of the week and represented as a function of the hour of the day of the Z component of the Cadí station for the 0.05-0.1 Hz frequency band (above left), 0.1-1 Hz (above right), 0.1-1 Hz (below left), and 10-40 Hz (below right).

[7] [8] [9]. These same timeframes also show elevated weekend amplitudes in the 10-40 Hz band, likely due to increased traffic through the Cadí Tunnel related to ski tourism, particularly during the February peak, which coincided with the season's highest recorded snow accumulation. Corresponding plots for the N and E components are available in the annex.

Figure 5 presents variations in seismic noise displacement for the Z component across several frequency bands. In the 0.05-0.1 Hz range, minimal variation is observed, as oscillations with periods over 10 seconds are uncommon. The 0.1-1 Hz band reveals lower amplitudes on Tuesdays, Wednesdays, and Thursdays. The 1-10 Hz range shows a displaced amplitude center, associated with global oceanic oscillations. As a result, amplitudes tend to be lower during nighttime and higher during the day throughout the week. The 10-40 Hz band clearly reflects anthropogenic noise: amplitudes drop significantly at night and on weekends, reflecting the general decrease in human activity. Equivalent plots for the N and E components are available in the annex.

C. Seismological events

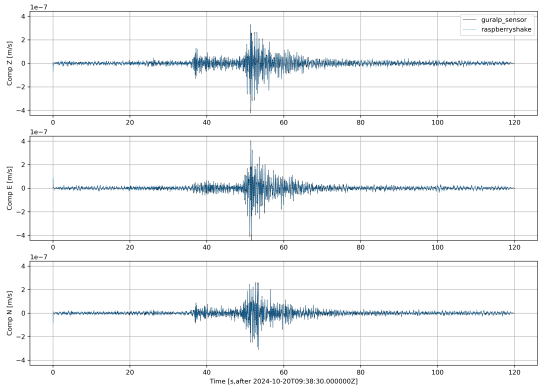

FIG. 6: Seismogram recorded at Cadí broadband station from the Empordà earthquake on 20-10-2024 at 09:38:46 UTC. Data provided by LEGEF-IEC. The plot shows ground motion in the Z, E, and N components, recorded by the Guralp sensor (line) and the Raspberry (dotted line). The time window displayed spans from 09:38:29 to 09:40:29 UTC. The trace has been bandpass filtered between 1 and 10 Hz to reduce ambient noise. Amplitudes in m/s and time in UTC.

Figures 6 7a 7b display seismograms recorded by both stations as examples of a local, a teleseismic, and a regional event, respectively. Both instruments effectively capture the local and regional earthquakes; however, only the Guralp broadband sensor registers the teleseism. In terms of amplitude, the raspberry sensor records approximately 10^{-8} whereas the Guralp sensor captures amplitudes around 10^{-6}, rendering the former as a faint line in the plots.

A comparison with data from other seismic stations within the CA seismic network [10] [11] [12], demonstrates that the Cadí station consistently and reliably detects these seismic events.

VI. CONCLUSIONS

In this study, the aim was to assess the data quality of the Cadí (LEGEC-IEC) broadband station. To that

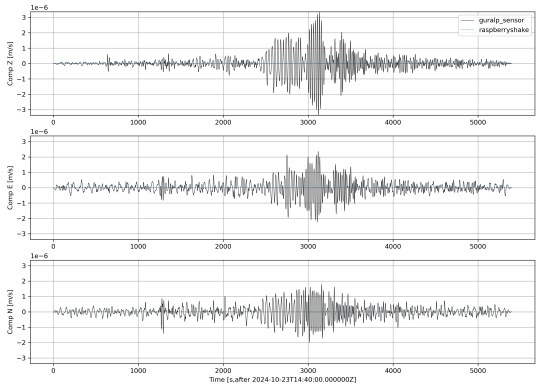

FIG. 7(a): Seismogram recorded at Cadí broadband station from the Russia earthquake on 23-10-2024 at 14:38:05 UTC. Data provided by LEGEF-IEC. The plot shows ground motion in the Z, E, and N components, recorded by the Guralp sensor (line) and the Raspberry (dotted line). The time window displayed spans from 14:40:00 to 16:10:00 UTC. The trace has been bandpass filtered between 0.01 and 0.1 Hz to reduce ambient noise. Amplitudes in m/s and time in UTC.

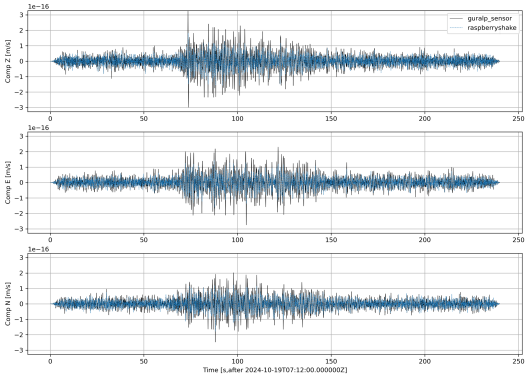

FIG. 7(b): Seismogram recorded at Cadí broadband station from the Crete earthquake on 19-10-2024 at 07:08:29 UTC. Data provided by LEGEF-IEC. The plot shows ground motion in the Z, E, and N components, recorded by the Guralp sensor (line) and the Raspberry (dotted line). The time window displayed spans from 07:11:59 to 07:15:59 UTC. The trace has been bandpass filtered between 0.01 and 0.1 Hz to reduce ambient noise. Amplitudes in m/s and time in UTC.

end, the cumulative PSD spectra, RMS amplitude, and temporal evolution of various seismic events recorded by the Cadí broadband station have been thoroughly analyzed in multiple formats and compared with data from other sources, including published studies and stations within the CA seismic network.

The results confirm that the Cadí (LEGEF-IEC) broadband station is indeed a well-performing installation. The cumulative PSD analysis shows that the station's data consistently fall within the NLNM and NHNM bounds and follow a pattern comparable to those of other reliable stations in the CA seismic network. Examination of the RMS amplitude plots across different frequency bands further indicates that the station's noise levels are stable and consistent over time, reinforcing the data quality. Lastly, the analysis of seismic event recordings, in comparison with both narrowband instrumentation and other CA network stations, verifies that the Cadí station operates reliably and accurately.

Future research could extend the analysis over a longer period of time to assess the station's long-term stability and seasonal variability, as well as a broader comparison with other stations in the CA Seismological Network to evaluate network-wide consistency.

Acknowledgments

I sincerely thank LEGEF-IEC and my advisors, Dr. Emma Suriñach and especially Dr. Mar Tapia, for her invaluable mentorship. I also appreciate the unwavering support of my friends, partner, and family.

[1] D. Mcnamara, Bulletin of the Seismological Society of America (2004), URL https://doi.org/10.1785/012003001.
[2] J. Peterson, U.S. Geological Survey (1993), URL https://doi.org/10.3133/ofr93322.
[3] J. Díaz and et al., Seismica (2025), URL https://doi.org/10.26443/seismica.v4i1.1408.
[4] T. Lecocq and et al., *Seismorms* (2020), URL https://github.com/ThomasLecocq/SeismoRMS.
[5] A. U. y Julio Mezcua, *Fundamentos de geofísica* (Alianza Editorial, 1997).
[6] J. Havskov and L. Ottemöller, *Routine Data Processing in Earth-quake Seismology* (Springer, 2010).
[7] *Butlletí climàtic anual del 2024*, URL https://static-m.meteo.cat/wordpressweb/wp-content/uploads/2025/04/17082331/BCA_2024-1.pdf.
[8] *Butlletí climàtic mensual gener del 2025*, URL https://static-m.meteo.cat/wordpressweb/wp-content/uploads/2025/02/20111731/BCM_2025_01.pdf.
[9] *Butlletí climàtic mensual febrer del 2025*, URL https://static-m.meteo.cat/wordpressweb/wp-content/uploads/2025/03/21095447/BCM_2025_02.pdf.
[10] *Detalls de l'esdeveniment 101300*, URL https://sismocat.icgc.cat/sisweb2/sisweb_details.php?lang=ca&codi=101300.
[11] *Detalls de l'esdeveniment 101354*, URL https://sismocat.icgc.cat/sisweb2/sisweb_details.php?lang=ca&codi=101354.
[12] *Detalls de l'esdeveniment 101324*, URL https://sismocat.icgc.cat/sisweb2/sisweb_details.php?lang=ca&codi=101324.

ESTUDI DE LES DADES SÍSMIQUES DE L'ESTACIÓ CADÍ (LEGEF-IEC) DE BANDA AMPLA

Júlia Ladero Gálvez
Facultat de Física, Universitat de Barcelona, Diagonal 645, 08028 Barcelona, Spain.

Advisors: Emma Suriñach, Mar Tapia

Resum: Verificar la qualitat de les dades enregistrades per les estacions sísmiques és essencial, especialment quan l'estació forma part d'una xarxa sísmica més àmplia. En aquest estudi, s'avalua la qualitat de les dades de l'estació de banda ampla del Cadí (LEGEC-IEC). Aquesta avaluació es duu a terme mitjançant l'elaboració, l'anàlisi i la comparació d'espectres de densitat espectral de potència (PSD) acumulats, valors d'amplitud quadràtica mitjana (RMS), i l'examen de diversos esdeveniments sísmics. Els resultats indiquen que les dades enregistrades presenten els patrons estacionals i en funció de la freqüència esperats, els nivells de soroll ambientals es mantenen dins dels límits acceptables, i l'estació registra de manera fiable esdeveniments sísmics globals. En conseqüència, es conclou que les dades generades per l'estació són de gran qualitat, consistents en el temps, i que l'estació funciona correctament.
Paraules clau: sismologia, banda ampla, anàlisi de dades, filtratge de dades
ODSs: Aquest TFG està relacionat amb l'ODS 13

Objectius de Desenvolupament Sostenible (ODSs o SDGs)

1. Fi de la es desigualtats	10. Reducció de les desigualtats	
2. Fam zero	11. Ciutats i comunitats sostenibles	
3. Salut i benestar	12. Consum i producció responsables	
4. Educació de qualitat	13. Acció climàtica	X
5. Igualtat de gènere	14. Vida submarina	
6. Aigua neta i sanejament	15. Vida terrestre	
7. Energia neta i sostenible	16. Pau, justícia i institucions sòlides	
8. Treball digne i creixement econòmic	17. Aliança pels objectius	
9. Indústria, innovació, infraestructures		

El contingut d'aquest TFG, part d'un grau universitari de Física, es relaciona amb l'ODS 13, ja que estudiant la banda atmosfèrica de freqüències de diferents PSDs al llarg dels anys es podria observar com ha afectat el canvi climàtic als fenòmens sismològics dins aquesta finestra.

A. SUPPLEMENTARY MATERIAL

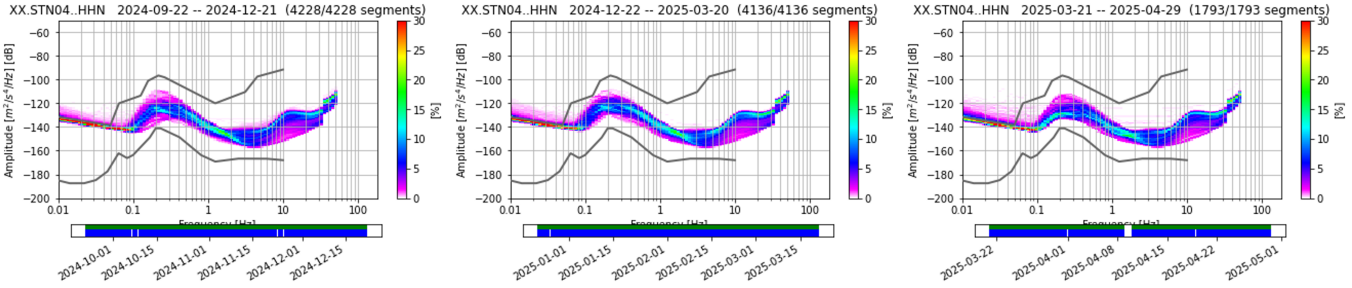

FIG. 1: Cumulative PSD spectra expressed in % for the N component. Every graphic corresponds to one season: autumn, winter, and spring, respectively. The grey curves are PSD spectra of the Earth's ambient seismic noise from [**?**]: upper (noisy) and lower (quiet). Data are expressed as dB relative to $1m^2\ s^{-4}\ Hz^{-1}$.

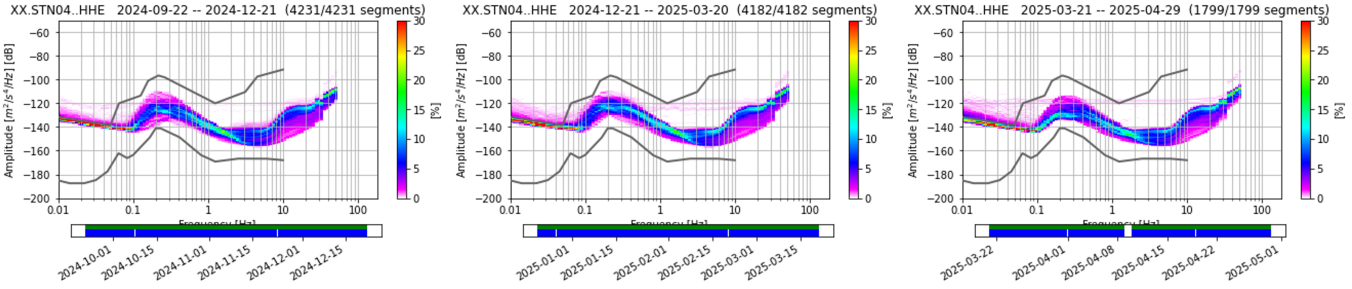

FIG. 2: Cumulative PSD spectra expressed in % for the E component. Every graphic corresponds to one season: autumn, winter, and spring, respectively. The grey curves are PSD spectra of the Earth's ambient seismic noise from [**?**]: upper (noisy) and lower (quiet). Data are expressed as dB relative to $1m^2\ s^{-4}\ Hz^{-1}$.

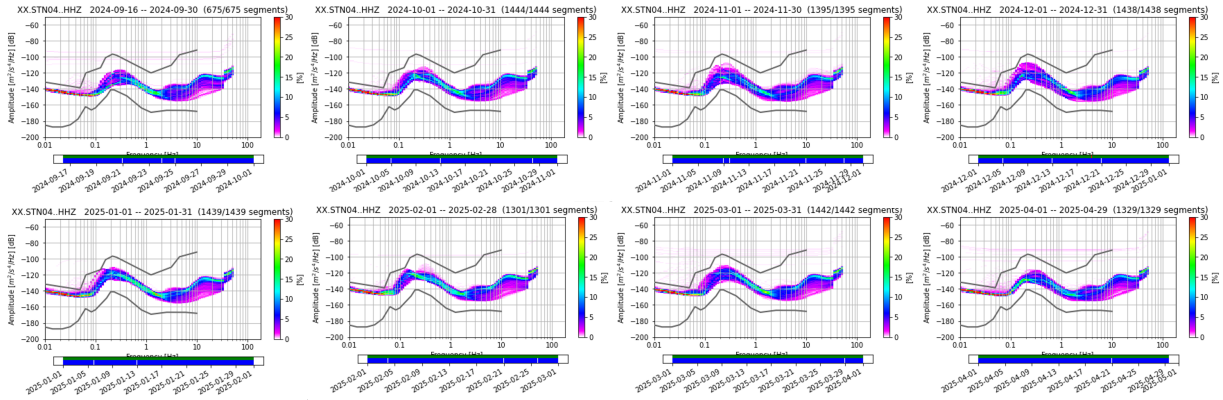

FIG. 3: Cumulative PSD spectra expressed in % for the Z component. Every graphic corresponds to one month from the analyzed data. The grey curves are PSD spectra of the Earth's ambient seismic noise from [**?**]: upper (noisy) and lower (quiet). Data are expressed as dB relative to $1m^2\ s^{-4}\ Hz^{-1}$.

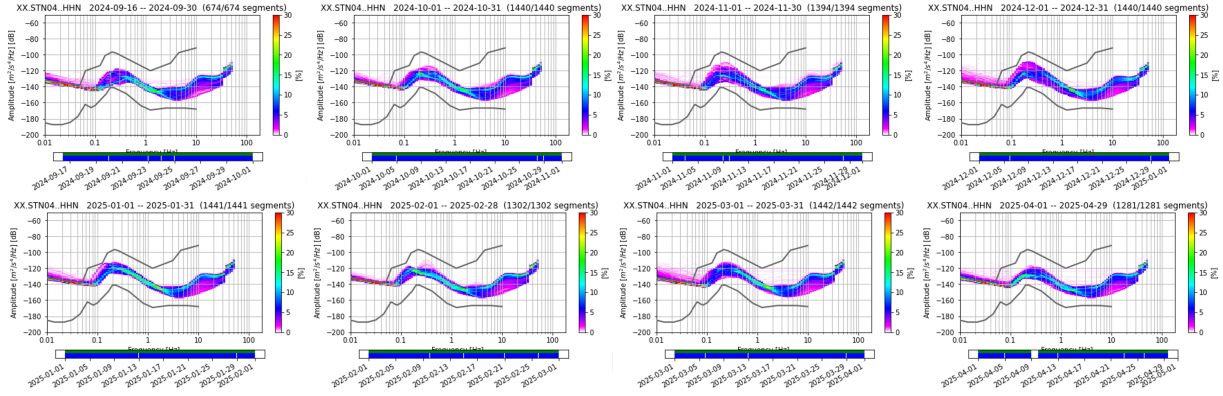

FIG. 4: Cumulative PSD spectra expressed in % for the N component. Every graphic corresponds to one month from the analyzed data. The grey curves are PSD spectra of the Earth's ambient seismic noise from [**?**]: upper (noisy) and lower (quiet). Data are expressed as dB relative to $1m^2\ s^{-4}\ Hz^{-1}$.

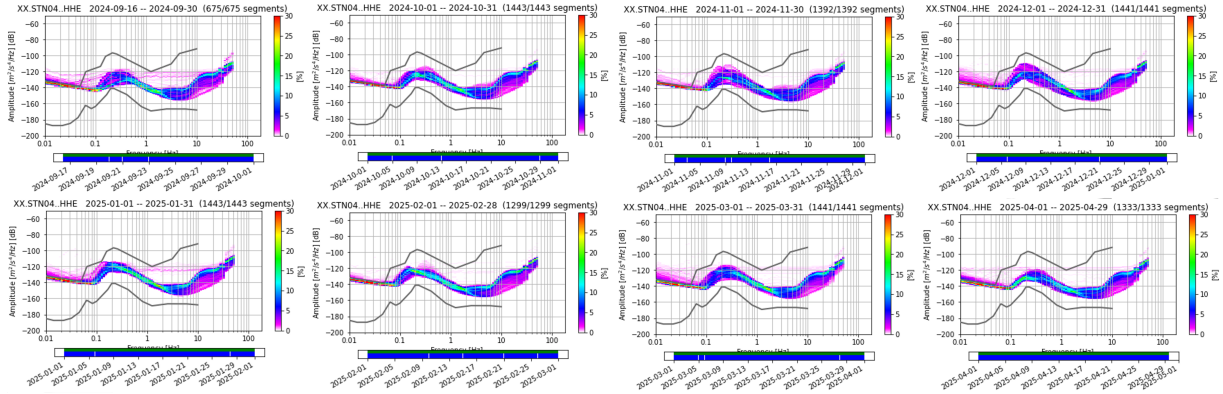

FIG. 5: Cumulative PSD spectra expressed in % for the E component. Every graphic corresponds to one month from the analyzed data. The grey curves are PSD spectra of the Earth's ambient seismic noise from [**?**]: upper (noisy) and lower (quiet). Data are expressed as dB relative to $1m^2\ s^{-4}\ Hz^{-1}$.

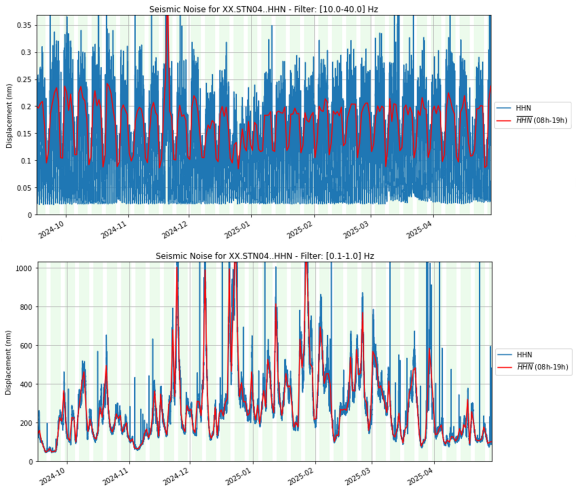

(a) Variations of the seismic noise displacement of the N component of the Cadí station for the 0.1-10 Hz frequency band (above) and 10-40 Hz (below). Blue line: displacement value averaged every 30 minutes. Red line: daily average of the shift of working and route hours (6h-19h UTC). Green background: working days (Monday to Friday). White background: weekend.

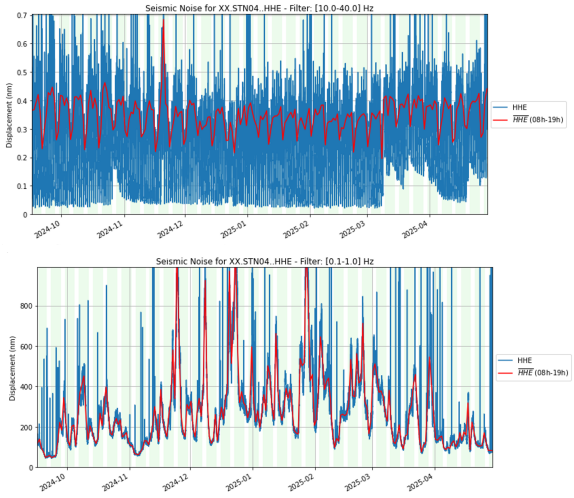

(b) Variations of the seismic noise displacement of the E component of the Cadí station for the 0.1-1 Hz frequency band (above) and 10-40 Hz (below). Blue line: displacement value averaged every 30 minutes. Red line: daily average of the shift of working and route hours (6h-19h UTC). Green background: working days (Monday to Friday). White background: weekend.

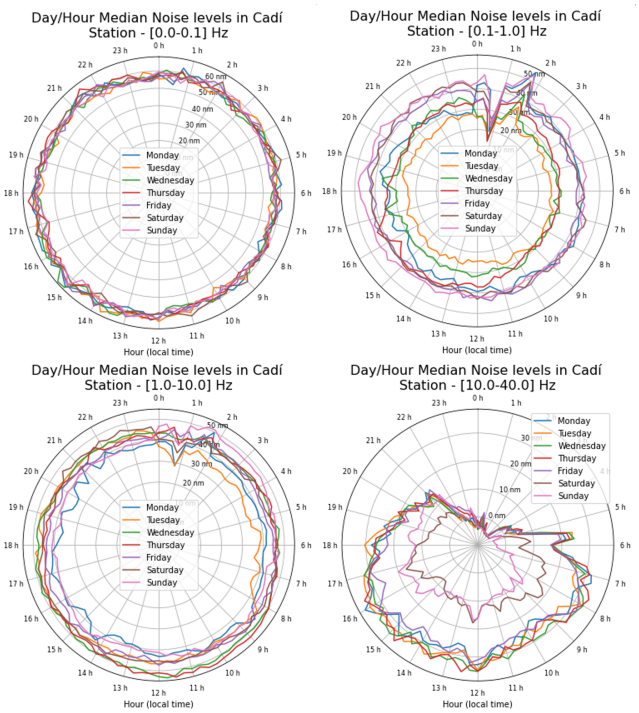

(a) Variations of the seismic noise displacement of the N component of the Cadí station for the 0.05-0.1 Hz frequency band (above left), 0.1-1 Hz (above right), 0.1-1 Hz (below left), and 10-40 Hz (below right). Data are divided by days of the week (Monday-Sunday) and represented based on time.

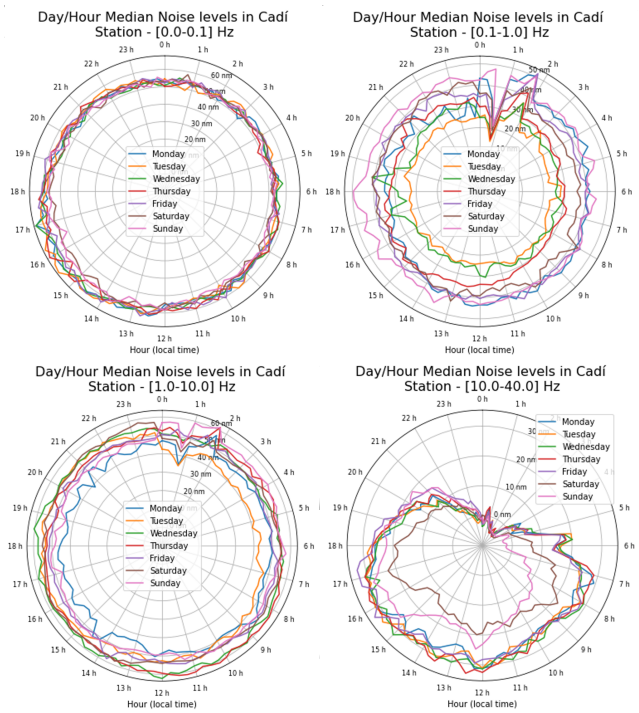

(b) Variations of the seismic noise displacement of the E component of the Cadí station for the 0.05-0.1 Hz frequency band (above left), 0.1-1 Hz (above right), 0.1-1 Hz (below left), and 10-40 Hz (below right). Data are divided by days of the week (Monday-Sunday) and represented based on time.

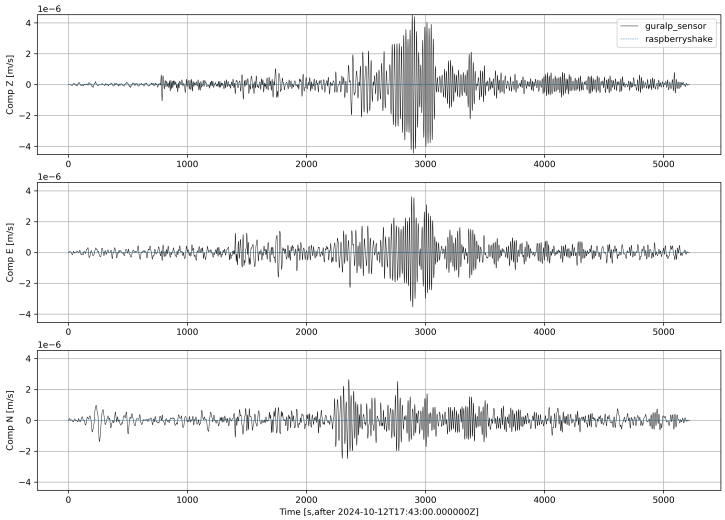

FIG. 8: Seismogram recorded at Cadí broadband station from the Costa Rica earthquake on 12-10-2024 at 17:43:45 UTC. The data were provided by LEGEF-IEC. The plot shows ground motion in the Z, E, and N components, recorded by the Guralp sensor (line) and the Raspberry (dotted line). The time window displayed spans from 17:42:59 to 19:09:59 UTC. The trace has been bandpass filtered between 0.01 and 0.1 Hz to reduce ambient noise. Amplitudes are shown in m/s, and time is given in UTC.